DRAFT VERSION SEPTEMBER 26, 2019
Typeset using LaTeX default style in AASTeX62

TYPE Ia SUPERNOVAE FROM NON-ACCRETING PROGENITORS

JOHN ANTONIADIS,[1,2] SAVVAS CHANLARIDIS,[2] GÖTZ GRÄFENER,[2] AND NORBERT LANGER[2,1]

[1]*Max-Planck Institut für Radioastronomie, Auf dem Hügel 69, 53121, Bonn DE*
[2]*Argelander Institut für Astronomie, Auf dem Hügel 71, 53121, Bonn DE*

Submitted to ApJ *Letters*

ABSTRACT

Type Ia supernovae (SNe Ia) are manifestations of helium-deficient stars disrupting in a thermonuclear runaway. While explosions of carbon-oxygen white dwarfs are thought to account for the majority of events, part of the observed diversity may be due to varied progenitor channels. We demonstrate that helium stars with masses between 1.8 and 2.5 $\mathrm{M}_\odot$ may evolve into highly degenerate, near-Chandrasekhar mass cores with helium-deficient envelopes, that subsequently ignite carbon and oxygen explosively at densities $\sim 10^{9.26-9.77}$ $\mathrm{gr\,cm^{-3}}$. This happens either due to compression from shell burning (when the core has a hybrid CO/NeO composition), or following ignition of residual carbon triggered by exothermic electron captures on $^{24}\mathrm{Mg}$ (for a NeOMg-dominated composition). We argue that the resulting thermonuclear runaways are likely to prevent core collapse, leading to the complete disruption of the star in a SN Ia explosion with a kinetic energy of $\sim 10^{51}$ erg. The frequency of progenitor systems would suffice to account for a large fraction of SNe Ia in star-forming galaxies.

Keywords: binaries: general - stars: evolution - supernovae: general

1. INTRODUCTION

Despite their central role in Astrophysics and Cosmology, the origin and physics of Type Ia supernovae (SNe Ia) remain uncertain (Maoz et al. 2014). Typical SN Ia luminosities ($\sim 10^{43}\,\mathrm{erg\,s^{-1}}$) and ejecta velocities ($\sim 10^{4}\,\mathrm{km\,s^{-1}}$), require $^{56}\mathrm{Ni}$ masses and kinetic energies of order $\sim 0.6\,\mathrm{M}_\odot$ and $\sim 10^{51}\,\mathrm{erg}$ respectively. These properties suggest that SNe Ia are most likely stars that disrupt in thermonuclear explosions, rather than core-collapse events. Carbon/oxygen white dwarfs (CO WDs) approaching the Chandrasekhar-mass limit (M_{Ch}) are the most promising progenitor systems, as they can produce explosions broadly consistent with observations (Nomoto 1982; Churazov et al. 2014).

Conventional stellar evolution channels, produce stable CO WDs with masses below $\sim 1.0\,\mathrm{M}_\odot$. Consequently, matter accretion onto the WD is required to trigger an explosion, either via stable transfer from a donor star (single-degenerate channels; SD), or in a merger event (double-degenerate channels; DD). Thus far, all of the proposed SD or DD variants encounter substantial difficulties in providing a self-consistent model for SNe Ia (Livio & Mazzali 2018). For instance, SD channels require considerable fine-tuning of the mass accretion rate for the WD to grow in mass. In addition, the interaction between the SN blast and the donor star or the circumbinary material, is expected to produce signatures which are rarely or never seen, e.g. some contribution to the SN luminosity at early times (Kasen 2010), radio synchrotron emission (Harris et al. 2016), and Hα lines due to unburned hydrogen. DD mergers on the other hand may produce a variety of outcomes, ranging from prompt explosions to long-lived remnants, or the delayed formation of a neutron star (Livio & Mazzali 2018). In addition, their overall contribution to the observed SN Ia rate may be too low (van Kerkwijk et al. 2010; Claeys et al. 2014a; Sato et al. 2015).

Over the past 50 years, systematic studies of SN Ia explosions have revealed a large diversity in their properties (Taubenberger 2017). Examples of extreme outliers include luminous (e.g. SN 1991T; Filippenko et al. 1992) and ultra-luminous (e.g. SNLS-03D3bb; Howell et al. 2006) SNe, SN 1991bg-like transients which are faint and rapidly evolving (Ruiz-Lapuente et al. 1993), and SN 2012ca-like events, dubbed SNe Ia-CSM, in which there is evidence for interaction with a dense circum-stellar medium

Corresponding author: John Antoniadis
janton@mpifr.de

(Bochenek et al. 2018). Even among "normal" SNe Ia there is appreciable scatter in rise times, maximum luminosities, ejecta velocities and spectral evolution (Livio & Mazzali 2018). Finally, there seems to be a correlation with environment, as active galaxies typically host more, and brighter SNe Ia (Maoz et al. 2014).

While part of this diversity can be understood within the framework of SD and DD families, there may exist additional evolutionary pathways leading to SNe Ia. Here, we explore an alternative channel in which a thermonuclear runaway leading to a SN Ia can be initiated during the late evolution of a degenerate core of neon-oxygen (NeO) or carbon-neon-oxygen (CNeO) composition that approaches $M_{\rm Ch}$. Such progenitors are generally thought to produce massive WDs or electron capture supernovae (ECSN) (e.g., Nomoto & Kondo 1991; Gutierrez et al. 1996; Takahashi et al. 2013). Here however, we show that near-$M_{\rm Ch}$ (C)NeO cores originating from intermediate mass helium stars ($\sim 1.8-2.5\,{\rm M}_\odot$) —a common product of binary interactions— can ignite their residual carbon and oxygen explosively at densities $\lesssim 10^{9.77}\,{\rm gr\,cm^{-3}}$, before the onset of ^{20}Ne(e$^-$,ν_e)^{20}Fe electron capture reactions (Section 2). In addition, the envelope is promptly lost via winds or due to binary interactions, leaving behind a helium-free structure. We demonstrate that the combination of final composition and available energy, would yield explosions with luminosities and ejecta velocities consistent with classical SNe Ia (Section 2.4). This mechanism does not require accretion from the binary companion and therefore may contribute significantly to the SN Ia rate in young stellar populations (Section 3).

2. (C)NeO CORES: FORMATION AND EVOLUTION

Highy degenerate stellar cores of neon-oxygen composition form inside stars with ZAMS masses between 7 and 11 ${\rm M}_\odot$ (Farmer et al. 2015; Woosley 2019). After core helium burning, such stars enter a super-asymptotic giant branch (SAGB) phase, characterized by a dense CO core and an extended hydrogen envelope. As the core becomes increasingly more degenerate, it cools substantially due thermal neutrino emission. An important consequence is that the critical temperature for ^{12}C ignition is first attained off-center, creating a convectively bound flame that propagates inwards (Siess 2006).

Carbon burning in SAGB stars is affected by complex mixing processes due to a combination of inverse composition gradients, overshooting, semi-convection and rotation. The penetration of NeONaMg ashes into unburned regions, may impact significantly the propagation of the burning front. Mixing generally reduces the thermonuclear reaction rate, leaving behind substantial amounts of residual carbon. In extreme cases, the flame can be quenched completely, resulting in a hybrid structure, with a CO core, surrounded by a NeO mantle (Denissenkov et al. 2013).

The subsequent evolution and final fate of the star depend critical on the competition between neutrino cooling due to the presence of ^{23}Na^{23}Ne and ^{25}Mg^{25}Na Urca pairs, and compressional heating due to accretion from the helium burning shell (Schwab et al. 2017). SAGB stars are subject to significant dredge-up and thermally unstable shell burning. These effects may impact substantially the ability of the core to grown in mass fast enough.

However, thermal pulses and dredge-up episodes do not occur when the hydrogen envelope is lost, e.g. due to a common envelope (CE) event in a binary system (Woosley 2019). In such a case, helium shell burning is stable, allowing the core to approach the Chandrasekhar mass limit. In what follows, we build detailed numerical models to investigate the combined effects of residual unburned ^{12}C, Urca cooling and constant mass accretion from shell burning, in the late evolution of (C)NeO cores that originate from helium stars.

2.1. *Numerical Calculations: Input Physics*

We use MESA version 10386 to follow the evolution of two helium-star models, M1 and M2, with masses of 2.4 and 1.8 ${\rm M}_\odot$ respectively. The initial models have uniform compositions with $Y = 0.98$ and $Z = 0.02$ (solar abundances are taken from Grevesse & Sauval 1998). We employ a nuclear network that considers 43 isotopes, from ^{1}H to ^{58}Ni. Reaction rates are based on the `JINA reaclib v2.0` compilation (Cyburt et al. 2010). Electron screening factors and cooling rates from thermal neutrinos are evaluated as in Farmer et al. (2015), and references therein. Weak interaction rates are taken from Suzuki et al. (2016). Wind mass loss rates are calculated using MESA's `Dutch` compilation (Paxton et al. 2013).

Our baseline convection model considers standard, thermohaline and semiconvectional mixing. Convective stability is evaluated using the Ledoux criterion. By default, MESA uses standard mixing-length theory (MTL; Cox & Giuli 1968) for convective mixing and energy transport. However, following carbon burning, both our models develop dynamically-unstable super-Eddington envelopes, causing numerical difficulties. For this reason, we decided to employ the "enhanced" MLT option available in MESA (Paxton et al. 2013), which artificially reduces the super-adiabatic gradient leading to an enhanced convective energy transport efficiency. This allows us to follow the evolution of the core after carbon burning without interruptions.We further discuss this choice and its impact on the envelope evolution and the final mass in Section 4. The MLT mixing length parameter is set to $a_{\rm MLT} = 2.0$ for both models. For thermohaline and semi-convection we employ the Kippenhahn et al. (1980) and Langer et al. (1983) treatments respectively. In addition to the baseline mixing parameters, in M2, we also consider the effects of

overshooting, adopting an efficiency of $f_{\rm ov} = 0.014$ across all convective boundaries, including the base of the carbon-burning flame. While mixing at this interface may not occur in reality, we use this as a means to quench the flame before reaching the center. Other mixing processes such as rotation and thermohaline can lead to the same outcome for similar initial helium core masses (Farmer et al. 2015). The MESA inlists are publicly available[1]. A more extended grid which explores a broad range of initial masses, metallicities and overshooting parameters will be presented in an accompanying paper (Chanlaridis et al. 2019).

2.2. *Simulation results*

Figure 1 shows Kippenhahn diagrams for M1 and M2, focusing on the evolution after central helium depletion. M1 first ignites

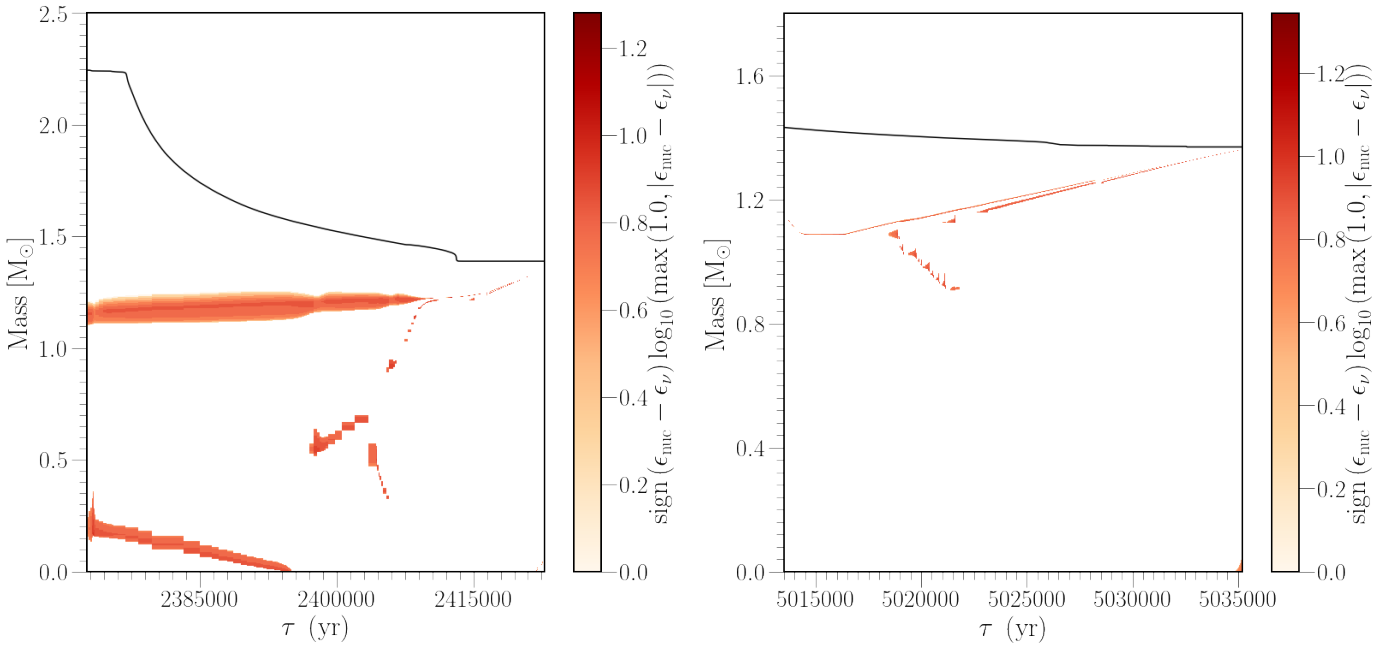

Figure 1. Kippenhahn diagrams following the evolution of M1 (left) and M2 after core helium depletion. Colored areas indicate regions in which nuclear burning occurs, i.e. locations for which the nuclear energy $\epsilon_{\rm nuc}$ exceeds energy losses due to neutrion emission, ϵ_ν.

carbon at mass coordinate $\sim 0.3\,{\rm M}_\odot$, when the total mass is $2.25\,{\rm M}_\odot$ and the CO core has a mass of $\sim 1.15\,{\rm M}_\odot$. The initial flame is followed by secondary flashes which propagate in both directions. Some of these episodes seem to occur only after a small critical mass of carbon has been accumulated below the burning shell. The entire carbon-burning phase lasts for about 40,000 yr. During most of this time, the star is a red giant with a low-density convective envelope ($R \simeq 125\,{\rm R}_\odot$, $\log_{10}(T_{\rm eff}/{\rm K}) \simeq 3.75$, $\log_{10}(L/\,{\rm L}_\odot) \simeq 4.3$), and loses mass at a rate of $\dot{M} \simeq 10^{-6}\,{\rm M}_\odot\,{\rm yr}^{-1}$, in good agreement with recent KEPLER models (Woosley 2019).

As the core contracts and its surface gravity increases, the surrounding burning shells become progressively thinner. The envelope responds by expanding and the stellar structure resembles closely that of an SAGB star. The last $\sim 5,000$ yr of the evolution are characterized by rigorous burning in two neighbouring shells which eventually merge, resulting in a ^{20}Ne flash. In this phase the star reaches extremely high luminosities up to $\log L/L_\odot = 6.25$ resulting in a strong stellar wind that lasts for $\sim$1000 yr and eventually removes the He-rich envelope.

The evolution of the envelope during the final stages depends critically on the energy transport mechanism above Eddington lumonisities. With the enhanced MLT option employed in our calculations, M1 briefly becomes a yellow supergiant as the envelope expands to $R \simeq 900\,{\rm R}_\odot$ while remaining dynamically stable. The strong wind of $\dot{M} \simeq 10^{-3.8}\,{\rm M}_\odot\,{\rm yr}^{-1}$ in this phase is in the same range as theoretically expected maximum values for super-Eddington winds (Owocki et al. 2004; Smith & Owocki 2006).

Conversely, using standard MLT, the envelope becomes dynamically unstable and our calculations encounter numerical difficulties just as the star leaves its Hayashi track, when the core has a mass of $1.32\,{\rm M}_\odot$. By extrapolating the core-growth rate,

[1] http://cococubed.asu.edu/mesa_market/inlists.html

the star would likely still reach the Chandrasekhar limit (see Woosley 2019, for a similar conclusion). More realistically, binary interactions would easily remove the envelope at this stage, as its binding energy corresponds to only a minuscule fraction of the orbital energy reservoir.

Interestingly, the combination of enhanced mass loss and vigorous burning, leads to the complete depletion of helium in the envelope. Following the thermal flash, the small residual envelope contracts and the wind ceases completely for the last ∼5,000 yr (Figure 1). Our model stops when the star has a mass of $1.39\,\mathrm{M}_\odot$ (see Sec. 2.3).

The surface evolution of M2 is similar (Figure 1). Here, the star expands twice, first for ∼5,000 yr, and then very briefly for some ∼500 yr, reaching a maximum size of $300\,\mathrm{R}_\odot$. The mass-loss rate however, always remains below $10^{-6}\,\mathrm{M}_\odot\,\mathrm{yr}^{-1}$. In M2, carbon ignites near mass coordinate $1\,\mathrm{M}_\odot$, just as the star begins to develop an SAGB structure. The flame is quenched after only $0.1\,\mathrm{M}_\odot$ of material has been converted to NeO, leaving behind a hybrid CO/NeO structure. Independently of whether this composition profile survives (Brooks et al. 2017), the amount of residual carbon is substantial. This model has a final mass of $1.37\,\mathrm{M}_\odot$.

To summarise, during the final evolutionary stages, both models are helium depleted and nearing $M_{\rm Ch}$. The ability of the core to grow in mass depends somewhat on the uncertain mass-loss rate during the final burning phases. If the envelope is lost too early during the SAGB phase (which does not seem to be the case), then the two stars would leave behind white dwarfs with masses $\leq 1.38\,\mathrm{M}_\odot$, and ONe and CO/ONe composition respectively.

Conversely, if the envelope is retained for long enough, then the central density increases sufficiently to trigger either electron captures on ^{24}Mg or central carbon ignition. In the following section we examine the evolution of the core during this phase.

2.3. *Late evolution and thermonuclear runaway*

Figure 2 gives an overview of the central density and temperature evolution for models M1 and M2 .

Following the main carbon-burning episode, both stars continue to contract, while cooling due to neutrino emission. As shell burning intensifies, compressional heating eventually balances off neutrino losses, at $\log_{10}(\rho_{\rm c}/\mathrm{gr\,cm^{-3}}) \simeq 8.3$ and 8.0 for M1 and M2 respectively. The subsequent evolution depends on the composition. For M1, the degenerate core is composed mostly of neon and oxygen. The most abundant isotopes have $X(^{16}\mathrm{O}) \simeq 0.43$; $X(^{20}\mathrm{Ne}) \simeq 0.42$; $X(^{24}\mathrm{Mg}) \simeq 0.1$; $X(^{12}\mathrm{C}) \simeq 0.011$; $X(^{23}\mathrm{Na}) \simeq 0.037$; $X(^{25}\mathrm{Mg}) \simeq 0.001$. Between $\log_{10}(\rho_{\rm c}/\mathrm{gr\,cm^{-3}}) = 9.05$ and 9.25, the temperature drops to $\log_{10}(T_{\rm c}/\mathrm{K}) \simeq 8.2$ due to ^{25}Mg^{25}Na and ^{23}Na^{23}Na direct Urca reactions. At higher densities, neutrino cooling ceases completely, and the temperature rises again, along the adiabatic curve shown in Figure 2.

When $\log_{10}(\rho_{\rm c}/\mathrm{gr\,cm^{-3}}) = 9.65$, exothermic electron captures on ^{24}Mg and ^{24}Na start occurring at a substantial rate, raising the temperature adequately to ignite carbon. In turn, this triggers oxygen burning and a thermonuclear runaway at $\log_{10}(\rho_{\rm c}/\mathrm{gr\,cm^{-3}}) = 9.77$. This ignition density is much lower than the $\log_{10}(\rho_{\rm c}/\mathrm{gr\,cm^{-3}}) \geq 9.97$ typically expected for oxygen deflagrations in pure NeO cores (Jones et al. 2019). As a consequence, severe deleptonization due to ^{20}Ne electron captures are avoided.

M2 is composed mostly of carbon and oxygen, with $X(^{12}\mathrm{C}) = 0.38$ and $X(^{16}\mathrm{O}) = 0.60$ respectively. Here, ^{23}Na is not abundant enough to cause substantial cooling. Consequently, carbon, which is significantly more abundant compared to M1, ignites at $\log_{10}(\rho_{\rm c}/\mathrm{gr\,cm^{-3}}) = 9.26$.

The evolution following central oxygen ignition is not adequately modeled in our 1D simulations. M2 will most likely disrupt in a SN Ia, as the composition and ignition conditions resemble closely those found in standard CO WD progenitors (Nomoto 1982). While the fate of M1 is less certain, a thermonuclear explosion is also the most likely outcome: firstly, the available nuclear energy is sufficient to unbind the star (see below). Secondly, the ignition density is not too much higher than the $\log_{10}(\rho_{\rm c}/\mathrm{gr\,cm^{-3}}) \simeq 9.3 - 9.7$ expected for CO WD progenitors. Hence, the deflagration ashes will likely be buoyant, leading to expansion, which will in turn limit the deleptonization rate. This hypothesis is strongly supported by 3D hydrodynamic simulations of ECSN deflagrations by Jones et al. (2019): their least compact progenitor ingites at $\log_{10}(\rho_{\rm c}/\mathrm{gr\,cm^{-3}}) = 9.90$ but still manages to eject $\sim 1\,\mathrm{M}_\odot$ of material. Similarly, Marquardt et al. (2015) simulate ONe WD detonations at lower densities and demonstrate that the explosion is practically identical to a typical SN Ia. Interestingly in our 1D simulations, both models experience significant expansion. This is most likely the result of (over-)efficient convection, which also homogenizes the inner $\sim 1\,\mathrm{M}_\odot$ of the core.

2.4. *Energetics and nucleosynthesis*

Figure 3 shows the density profiles of M1 and M2 at maximum compactness, and at the end of our simulations. At the onset of oxygen ignition, M1 and M2 have internal energies (gravitational+thermal) of -5.76 and -5.16 erg, and average electron fractions of $Y_e = 0.496$ and 0.499 for M1 and M2 respectively. If these progenitors were to produce an SN Ia of typical

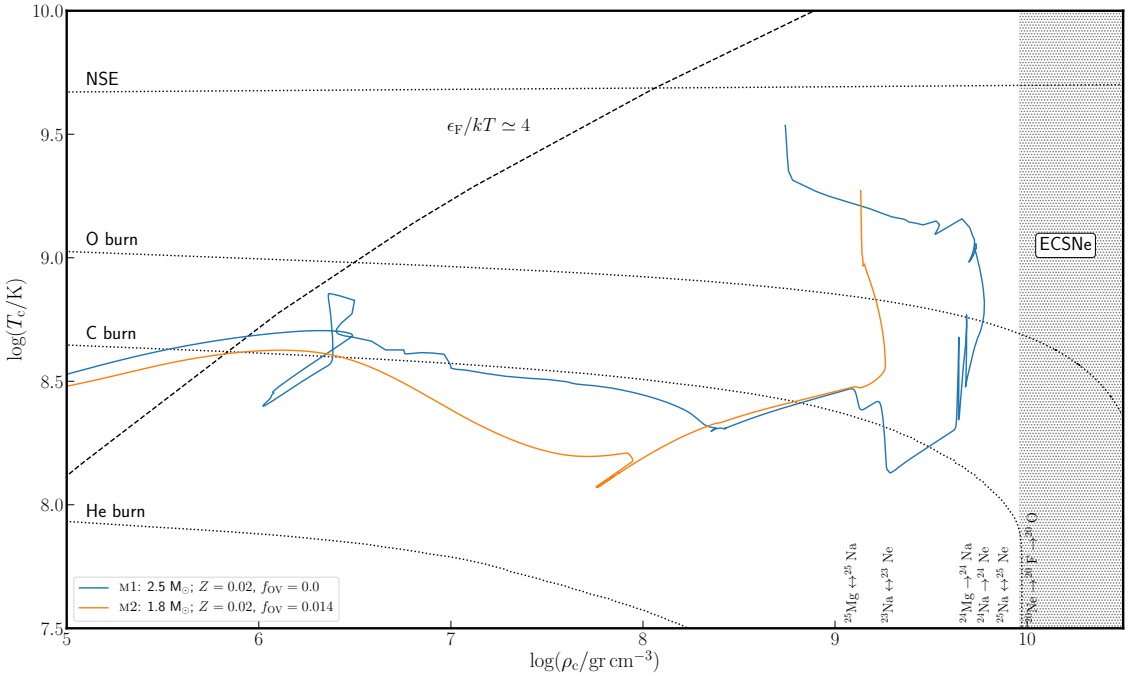

Figure 2. Evolution of the core density and temperature for M1 and M2. The dashed line shows the approximate boundary for electron degeneracy. Burning thresholds for a 100% abundace of the corresponding species are indicated with dotted lines. The NSE threshold assumes an equilibrium timescale of 1 s.

composition of $\sim 0.7\,\mathrm{M}_\odot$ of nickel and iron and $0.6\,\mathrm{M}_\odot$of Si-group elements, the corresponding kinetic energies would be $E_{\mathrm{M1}} \simeq 0.83$ and $E_{\mathrm{M2}} \simeq 1.17 \times 10^{51}$ erg, consistent with observations. Obviously, the nucleosynthesis yields depend on the actual Y_e and density profiles during explosive burning. If M1 achieves nuclear statistical equilibrium (NSE) without significant expansion and deleptonization, then it would produce mostly stable iron-peak elements and $\sim 0.3\,\mathrm{M}_\odot$ of ^{56}Ni, resulting in a sub-luminous explosion. On the other hand, if NSE is achieved after an initial deflagration (Figure 3), then up to $1\,\mathrm{M}_\odot$ of ^{56}Ni can be produced, with only moderate amounts of iron. Similarly, M2 could produce up to $1.3\,\mathrm{M}_\odot$ of iron elements if it doesn't expand any further.

3. EXPECTED RATES AND DELAY TIMES

A useful proxy for the potential (C)NeO/SN Ia connection would be a comparison between the Hubble-integrated number of SNe Ia, $\mathrm{n_{SN\,Ia}}$, and the expected frequency of stripped near-Chandrasekhar mass (C)NeO cores, $n_\star$. Here, we provide an order-of-magnitude estimate to demonstrate that the two may indeed be similar.

To first order, $n_\star$ would be some fraction of the initial star-forming mass that will end up creating (C)NeO cores. Since the envelope needs to be removed before the onset of core helium burning, these stars would also need to be members of close binary systems, thus:

$$n_\star \simeq f_{\mathrm{bin}} \times f_{\mathrm{int}} \times n_{\mathrm{(C)NeO}}. \tag{1}$$

Here, $f_{\mathrm{bin}} \simeq 0.7$ (Sana et al. 2012) is the stellar binary fraction, $n_{\mathrm{(C)NeO}}$ is the total number of stars able to form (C)NeO cores, and $f_{\mathrm{int}} \leq 1$ is an efficiency factor to account for the impact of binary interactions (see below).

For binaries, the number of systems with ZAMS masses within a certain range (Figure 4) is:

$$n(m_1, m_2) dm_1 dm_2 = m_1^\alpha q^\kappa dm_1 dq, \tag{2}$$

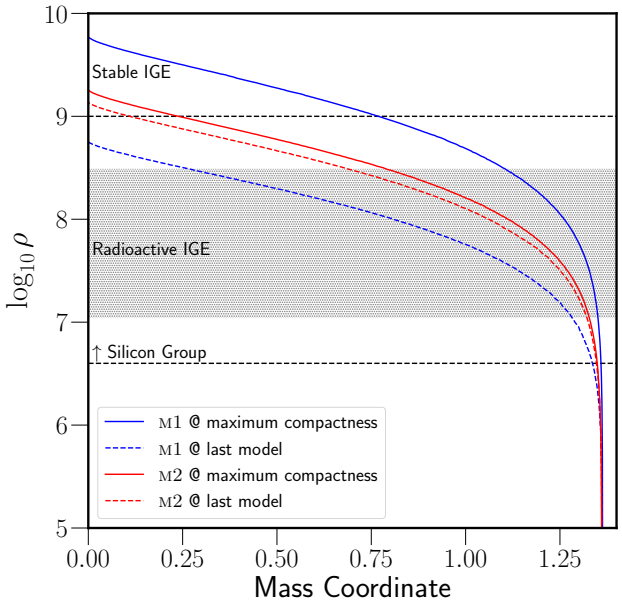

Figure 3. Density profiles at maximum compactness (solid lines) and at the end of our MESA calculations (dashed lines). Regions indicating approximate burning regimes as in Seitenzahl & Townsley (2017).

where m_1 is the mass of the primary, here defined as the initially more massive star, $q \equiv m_2/m_1 \leq 1$ is the mass ratio, and a, κ depend on the initial mass function (IMF) and mass-ratio distribution respectively. Integrating, one finds:

$$N = \int_{m_{\rm min}}^{m_{\rm max}} \int_{q_1}^{q_2} m_1^{\alpha} q^{\kappa} dm_1 dq = f \frac{(m_{\rm min}^{\alpha+1} - m_{\rm max}^{\alpha+1})(q_1^{\kappa+1} - q_2^{\kappa+1})}{(\alpha+1)(\kappa+1)}, \tag{3}$$

where f is an appropriate normalization factor. Naively, one would expect the largest contribution from stars that, in isolation, would be able to evolve to the SAGB, viz. stars with ZAMS masses between $\sim$ 7 and 11 $\rm M_\odot$ (Farmer et al. 2015). Since accretion is not required to trigger an explosion, *all* primaries and secondaries inside this mass range can potentially contribute to $n_\star$. Hence, $(m_{\rm min}, m_{\rm max}) = (7, 11)\,\rm M_\odot; (q_1, q_2) = (0, 1)$ for the primaries (blue region in Figure 4), and $(m_{\rm min}, m_{\rm max}) = (11, 125)\,\rm M_\odot; (q_1, q_2) = (7/11, 1)$ for the secondaries (red region). For normalization, we consider all systems within $(m_{\rm min}, m_{\rm max}) = (0.1, 125)\,\rm M_\odot$. Adopting a Chabrier (2005) IMF with $a = -2.35$ for $m_1 \geq 1$, and a $q-$distribution with $k = -0.1$ (Sana et al. 2012), Eq. 3 yields, $n_{\rm (C)NeO} \times f_{\rm bin} \simeq 5.42 \times 0.7 = 0.0039$ stars per $\rm M_\odot$ formed, with the largest contribution ($\sim 80\%$) expected from primaries. For $f_{\rm int} \simeq 1$, $n_\star$ would therefore exceed the number of SN Ia integrated over a Hubble time, $n_{\rm SN\,Ia} \simeq 0.002\,\rm M_\odot{}^{-1}$ (Maoz et al. 2014).

However, $f_{\rm int}$ is most likely smaller than unity. Firstly, only a fraction of the progenitor binary population will create naked helium stars. Most systems within the hatched regions of Figure 4 will transfer mass to their less massive companions after leaving the main sequence. For the majority of these cases, this process will be dynamically unstable, therefore leading to the removal of the envelope. If this process is indeed efficient, one would expect at least half of the stars to lose their envelopes, hence, conservatively, $f_{\rm int} \lesssim 0.5$ (Sana et al. 2012).

Following the stripping of the envelope, any subsequent interaction should be sufficiently delayed, for the core to reach $M_{\rm Ch}$. The post-CE orbital period distribution would generally favor slightly more compact configurations. Hence, only some fraction of the systems will be wide enough to allow a second CE episode after the progenitor has expanded beyond $\sim 100\,\rm R_\odot$. Nonetheless, a fraction of the closer binaries that will undergo stable case BB Roche-lobe overflow (RLO), could still leave behind stripped (C)NeO cores of sufficiently high mass. For instance, the simulations of Tauris et al. (2015) suggest that a considerable number of helium-free (C)NeO proto-WDs with $m \simeq M_{\rm Ch}$ can be produced via this channel.

Considering some of the major uncertainties, conservatively, we expect: $0.1 \lesssim f_{\rm int} \lesssim 0.5$. Taking into account further ambiguities in the IMF and initial configurations, we conclude that $0.05 \lesssim n_\star/n_{\rm SN\,Ia} \lesssim 1$.

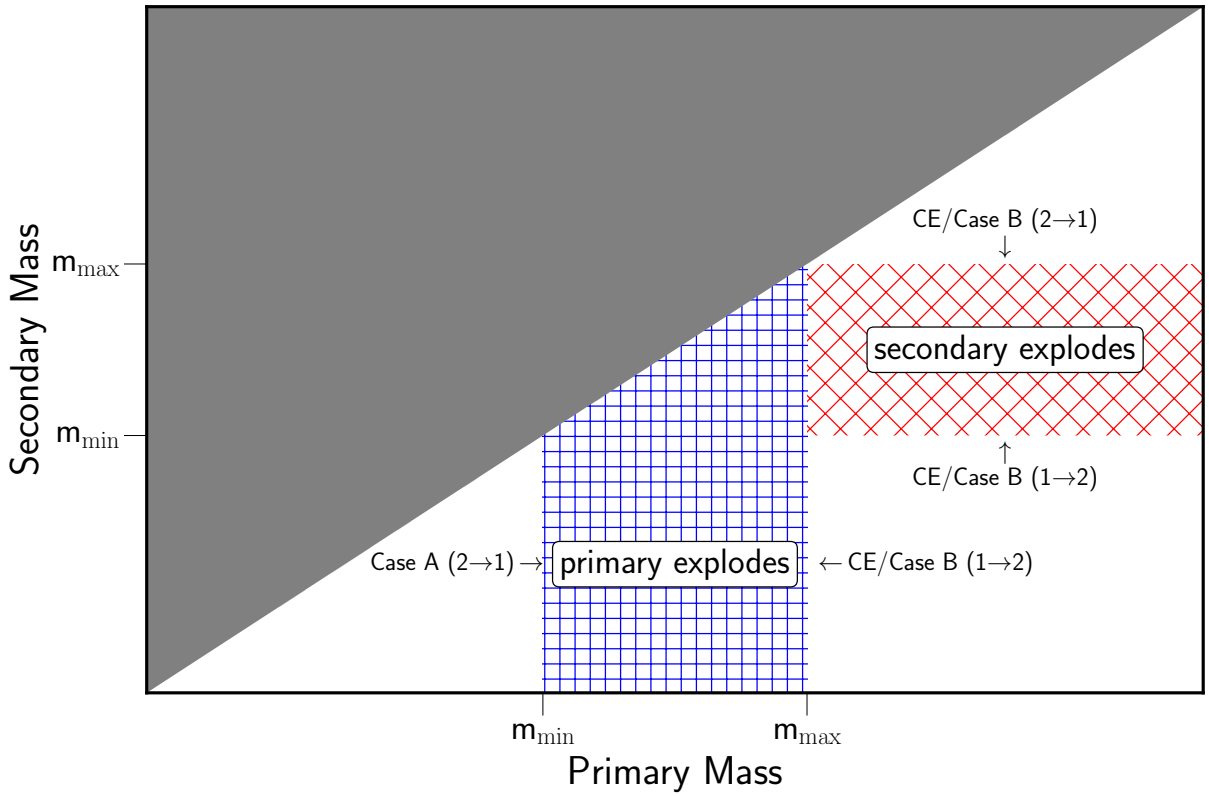

Figure 4. Overview of the different systems contributing to the SN Ia channel discussed here, on the mass-mass plane (see text).

Obviously, the above estimate omits most interactions that could move systems in and out of the hatched regions in Figure 4. Of particular importance may be interactions occurring before the helium-burning phase, as there are roughly three times as many systems with a total mass larger than $7\,\mathrm{M}_\odot$ than there are stars within the hatched regions of Figure 4. A fraction of this population can contribute significantly to the observed rate, after interacting via Case A/B RLO. Additional contributions may come from higher-order multiple systems and/or dynamical interactions in dense environments.

Besides the integrated number of SNe Ia, a property that is more challenging to match is the evolution of the SN Ia rate with cosmic time. SNe Ia from this channel would have delay times dominated by the main sequence lifetime of the progenitors, i.e. of order 25 to 78 Myr, for stars with ZAMS masses between 7 and $11\,\mathrm{M}_\odot$. Binaries interacting via early Case A RLO prior to the removal of the envelope, could contribute events up to ~ 350 Myr following star formation.

These delay times could help account for the high SN Ia rates in star-forming galaxies (Maoz & Badenes 2010; Claeys et al. 2014b). However, some variant of the DD channel would still be required to explain events with much longer delay times.

4. SUMMARY

We have shown that stars able to form degenerate (C)NeO cores after losing their hydrogen envelopes, are likely to explode as SNe Ia instead of undergoing a core-collapse ECSN. For NeO compositions, the runaway seems to be triggered by the ignition of residual carbon following electron captures on ^{24}Mg, which in turn leads to explosive oxygen burning at densities below $10^{9.77}\,\mathrm{gr\,cm^{-3}}$ (Sections 2). For hybrid CO/NeO cores, ignition is triggered by core compression, at a density of $10^{9.26}\,\mathrm{gr\,cm^{-3}}$, similar to what is expected for CO WD deflagrations. For either case, the conditions at the onset of oxygen burning are such that the energetics could resemble closely a typical SNe Ia (Section 2.4). It would be worth considering whether the differences in density and composition could lead to distinct nucleosynthetic signatures that would help distinguish these progenitors and/or contribute uniquely to the chemical evolution of the Galaxy (in analogy to Jones et al. 2019, for ECSNe).

The frequency of the corresponding progenitor systems is sufficient to account for a considerable fraction of the observed SN Ia rate (Section 3). Since, the bulk of events would occur only ~ 50 Myr after star formation, this channel is mostly relevant to active late-type galaxies. The shorter delay times compared to traditional SN Ia scenarios, opens further interesting avenues for constraining this model, e.g. with low-metallicity stars.

A similar SN Ia channel has been proposed by Waldman & Barkat (2006) and Waldman et al. (2008), who have also demonstrated that some helium stars with (C)NeO cores can explode before any significant deleptonization occurs. However, these authors do not follow the final evolution stages, and their progenitors still retain a small He-rich envelope at the end. While here we demonstrate that the helium envelope is likely lost only after the core has grown to $M_{\rm Ch}$, its evolution remains a major uncertainty for this progenitor channel. If helium is removed sufficiently early, e.g. due to binary interactions or dynamical instabilities, then this channel would instead create sub-$M_{\rm Ch}$ (C)NeO WDs. In spite of the mass-loss uncertainties, if viable, this channel would help explain some of the observed SN Ia diversity. Since either star in binary system may potentially explode as a SN Ia without accreting from its companion, the resulting events can resemble setups expected in both SD and DD scenarios. Explosions resulting from the explosion of the secondary, would follow a first core-collapse SN. This could lead to SN Ia remnants with no luminous surviving stars, high proper motions due to a kick from the first SN (like the Kepler remnant, Chiotellis et al. 2012), and possibly associated with a neutron star. Since the envelope can be removed either due to winds, case-BB mass transfer, or a common envelope event, some diversity is also expected in the SN environment. In turn this would influence bot the appearance of the explosion and the evolution of the SN remnant.

Finally this channel seems relevant to other emerging correlations, e.g. the one found between SN locations and the velocity of Si features, or the apparent correlation between SN Ia rate and IMF variations at low masses (Maoz et al. 2014).

We thank Philipp Podsiadlowski, Friedrich Röpke, Samuel Jones and Josiah Schwab for useful discussions. This research made extensive use of NASA's ADS.

Software: MESA[2] (Paxton et al. 2011, 2013, 2015, 2018), Astropy[3] (Astropy Collaboration & Astropy Contributors 2018) , MESAplot (Farmer 2018)

REFERENCES

Astropy Collaboration, & Astropy Contributors. 2018, The Astronomical Journal, 156, 123

Bochenek, C. D., Dwarkadas, V. V., Silverman, J. M., et al. 2018, Monthly Notices of the Royal Astronomical Society, 473, 336

Brooks, J., Schwab, J., Bildsten, L., Quataert, E., & Paxton, B. 2017, The Astrophysical Journal, 834, L9

Chabrier, G. 2005, The Initial Mass Function 50 Years Later, 327, 41

Chanlaridis, S., Antoniadis, J., Gräfener, G., & Langer, N. 2019, in prep.

Chiotellis, A., Schure, K. M., & Vink, J. 2012, Astronomy & Astrophysics, 537, A139

Churazov, E., Sunyaev, R., Isern, J., et al. 2014, Nature, 512, 406

Claeys, J. S. W., Pols, O. R., Izzard, R. G., Vink, J., & Verbunt, F. W. M. 2014a, Astronomy & Astrophysics, 563, A83

—. 2014b, Astronomy and Astrophysics, 563, A83

Cox, J. P., & Giuli, R. T. 1968, Principles of stellar structure

Cyburt, R. H., Amthor, A. M., Ferguson, R., et al. 2010, The Astrophysical Journal Supplement Series, 189, 240

Denissenkov, P. A., Herwig, F., Truran, J. W., & Paxton, B. 2013, The Astrophysical Journal, 772, 37

Farmer, R. 2018, rjfarmer/mesaplot

Farmer, R., Fields, C. E., & Timmes, F. X. 2015, The Astrophysical Journal, 807, 184

Filippenko, A. V., Richmond, M. W., Matheson, T., et al. 1992, The Astrophysical Journal, L5

Grevesse, N., & Sauval, A. J. 1998, Space Science Reviews, 85, 161

Gutierrez, J., Garcia-Berro, E., Iben, I., et al. 1996, The Astrophysical Journal, 459, 701

Harris, C. E., Nugent, P. E., & Kasen, D. N. 2016, The Astrophysical Journal, 823, 100

Howell, D. A., Sullivan, M., Nugent, P. E., et al. 2006, Nature, 443, 308

Jones, S., Röpke, F. K., Fryer, C., et al. 2019, Astronomy and Astrophysics, 622, A74

Kasen, D. 2010, The Astrophysical Journal, 708, 1025

Kippenhahn, R., Ruschenplatt, G., & Thomas, H.-C. 1980, Astronomy and Astrophysics, 91, 175

Langer, N., Fricke, K. J., & Sugimoto, D. 1983, Astronomy and Astrophysics, 126, 207

Livio, M., & Mazzali, P. 2018, Physics Reports, 736, 1

[2] http://mesastar.org
[3] http://www.astropy.org

Maoz, D., & Badenes, C. 2010, Monthly Notices of the Royal Astronomical Society, 407, 1314

Maoz, D., Mannucci, F., & Nelemans, G. 2014, Annual Review of Astronomy and Astrophysics, 52, 107

Marquardt, K. S., Sim, S. A., Ruiter, A. J., et al. 2015, Astronomy and Astrophysics, 580, A118

Nomoto, K. 1982, The Astrophysical Journal, 253, 798

Nomoto, K., & Kondo, Y. 1991, The Astrophysical Journal, 367, L19

Owocki, S. P., Gayley, K. G., & Shaviv, N. J. 2004, The Astrophysical Journal, 616, 525

Paxton, B., Bildsten, L., Dotter, A., et al. 2011, The Astrophysical Journal Supplement Series, 192, 3

Paxton, B., Cantiello, M., Arras, P., et al. 2013, The Astrophysical Journal Supplement Series, 208, 4

Paxton, B., Marchant, P., Schwab, J., et al. 2015, The Astrophysical Journal Supplement Series, 220, 15

Paxton, B., Schwab, J., Bauer, E. B., et al. 2018, The Astrophysical Journal Supplement Series, 234, 34

Ruiz-Lapuente, P., Jeffery, D. J., Challis, P. M., et al. 1993, Nature, 365, 728

Sana, H., de Mink, S. E., de Koter, A., et al. 2012, Science, 337, 444

Sato, Y., Nakasato, N., Tanikawa, A., et al. 2015, The Astrophysical Journal, 807, 105

Schwab, J., Bildsten, L., & Quataert, E. 2017, Monthly Notices of the Royal Astronomical Society, 472, 3390

Seitenzahl, I. R., & Townsley, D. M. 2017, Nucleosynthesis in Thermonuclear Supernovae, 1955

Siess, L. 2006, Astronomy and Astrophysics, 448, 717

Smith, N., & Owocki, S. P. 2006, ApJL, 645, L45

Suzuki, T., Toki, H., & Nomoto, K. 2016, \apj, 817, 163

Takahashi, K., Yoshida, T., & Umeda, H. 2013, The Astrophysical Journal, 771, 28

Taubenberger, S. 2017, Handbook of Supernovae, 317

Tauris, T. M., Langer, N., & Podsiadlowski, P. 2015, Monthly Notices of the Royal Astronomical Society, 451, 2123

van Kerkwijk, M. H., Chang, P., & Justham, S. 2010, The Astrophysical Journal, 722, L157

Waldman, R., & Barkat, Z. 2006, Ph.D. Thesis

Waldman, R., Yungelson, L. R., & Barkat, Z. 2008, in Astronomical Society of the Pacific Conference Series, Vol. 391, Hydrogen-Deficient Stars, ed. A. Werner & T. Rauch, 359

Woosley, S. E. 2019, The Astrophysical Journal, 878, 49